2018

A Novel Transgenic Rat Model of Robust Cerebral Microvascular Amyloid with Prominent Vasculopathy

Judianne Davis
University of Rhode Island, judiannedavis@uri.edu

Feng Xu
University of Rhode Island, feng_xu@uri.edu

See next page for additional authors

Citation/Publisher Attribution
Davis, J., Xu, F., Hatfield, J., Lee, H., Hood, M. D., Popescu, D.,...Van Nostrand, W. E. (2018). A Novel Transgenic Rat Model of Robust Cerebral Microvascular Amyloid with Prominent Vasculopathy. *The American Journal of Pathology, 188*(12), 2877-2889. doi: 10.1016/j.ajpath.2018.07.030
Available at: http://dx.doi.org/10.1016/j.ajpath.2018.07.030

Section: Animal Models

A Novel Transgenic Rat Model of Robust Cerebral Microvascular Amyloid with Prominent Vasculopathy

Judianne Davis*, Feng Xu*, Joshua Hatfield*, Hedok Lee¶, Michael D. Hoos§, Dominique Popescu#, Elliot Crooks§, Regina Kim*, Steven O. Smith§, John K. Robinson*,†, Helene Benveniste¶, and William E. Van Nostrand*,∫

George & Anne Ryan Institute for Neuroscience*
Department of Psychology†
Department of Biomedical & Pharmaceutical Sciences∫
University of Rhode Island
Kingston, RI 02881

Departments of Psychology# and Biochemistry & Cell Biology§
Stony Brook University
Stony Brook, NY 11794

Department of Anesthesiology¶
Yale University
New Haven, CT

Address correspondence to: Dr. William E. Van Nostrand
George & Anne Ryan Institute for Neuroscience
University of Rhode Island
130 Flagg Road
Kingston, RI 02881
E-mail: wvannostrand@uri.edu

Pages: *38*
Figures: *8*
Running title: *Transgenic Rat Model of CAA*

This work was supported by NIH grants NS091969 (WVN,JR,HB), AG053991 (HB,WVN) and NS092696 (WVN,SS).

Disclosures: None declared.

Abstract

Accumulation of fibrillar amyloid β-protein (Aβ) in blood vessels of the brain, a condition known as cerebral amyloid angiopathy (CAA), is a common pathology of the elderly, a prominent comorbidity of Alzheimer's disease and driver of vascular cognitive impairment and dementia (VCID). Although several transgenic mouse lines have been generated that develop varying levels of CAA, consistent models of associated cerebral microhemorrhage and vasculopathy observed clinically have been lacking. Reliable preclinical animal models of CAA and microhemorrhage are needed to investigate the molecular pathogenesis of this condition. Here, we describe the generation and characterization of a novel transgenic rat (rTg-DI) that produces low levels of human familial CAA Dutch/Iowa E22Q/D23N mutant Aβ in brain and faithfully recapitulates many of the pathological aspects of human small vessel CAA. rTg-DI rats exhibit early-onset and progressive accumulation of cerebral microvascular fibrillar amyloid accompanied by early-onset and sustained behavioral deficits. Comparable to CAA in humans, the cerebral microvascular amyloid in rTg-DI rats causes capillary structural alterations, promotes prominent perivascular neuroinflammation and produces consistent, robust microhemorrhages and small vessel occlusions that are readily detected by magnetic resonance imaging. The rTg-DI rats provide a new model to investigate the pathogenesis of small vessel CAA and microhemorrhages, to develop effective biomarkers for this condition and to test therapeutic interventions.

Introduction

Cerebral amyloid angiopathy (CAA) is a common cerebral small vessel disease that involves the accumulation of amyloid β-protein (Aβ) primarily in small- and medium-sized arteries and arterioles of the meninges and cerebral cortex as well as along the capillaries of the cerebral microvasculature [1-6]. CAA has been shown to be present, in varying degrees, in nearly 80% of elderly individuals [7,8]. With the involvement of Aβ, it is not surprising that CAA is a very common vascular comorbidity in patients with Alzheimer's disease (AD) [3,7-9]. Even when controlling for confounders including AD, CAA is a significant contributor to vascular-mediated cognitive impairment and dementia (VCID) and is independently associated with worse cognition and dementia [7,8,10-13]. In addition to the sporadic cases of CAA and the prominent CAA that is observed in AD, several monogenic, familial forms of CAA exist that result from mutations that reside within the Aβ peptide sequence of *APP* gene including the Dutch E22Q and Iowa D23N variants [12-14].

CAA can present as two prominent forms known as CAA type-1 and CAA type-2 [6]. In CAA-type 2 the amyloid deposition is largely restricted within the vessel wall of the meningeal and cortical arterioles and generally does not promote perivascular neuroinflammation [5,6,15]. In contrast, CAA type-1 involves amyloid deposition along transitional cerebral microvessels and capillaries and is present in nearly half of AD cases [5,6]. In contrast to larger vessel CAA type-2 where the amyloid is largely confined within the vessel wall, CAA type-1 results in penetrance of the fibrillar amyloid deposits into the surrounding brain parenchyma – so called "dyshorric amyloid" – a feature which promotes a strong perivascular neuroinflammatory response [5,6,16,17]. In particular, cerebral

microvascular amyloid deposition is often correlated with worse cognition and dementia in individuals afflicted with AD and sporadic/familial CAA disorders [18-22].

Transgenic mice, which robustly over-express human AβPP in brain and develop cerebral Aβ deposits, have been a significant advancement for the study of the pathogenic effects of brain Aβ accumulation *in vivo*. Several well-established transgenic mouse lines have been developed that over-produce human Aβ peptides in brain that develop age-dependent accumulation of parenchymal Aβ deposits with varying degrees of CAA and associated vasculopathies [23-26]. Specifically, transgenic mouse lines were developed that express human AβPP in brain harboring one or more of the familial CAA mutations [27,28]. Importantly, these familial CAA transgenic mouse lines revealed the specific role of CAA in neuroinflammation and VCID [29-32]. However, as with all mouse models, CAA transgenic mice possess some significant limitations to more fully recapitulate and study the equivalent human condition. In particular, consistent and robust microbleeds have been elusive in most CAA mouse models. Therefore, more appropriate animal models of small vessel CAA are necessary to progress our understanding of the pathogenesis, its contribution to structural changes in the brain and VCID.

Here we describe our efforts to generate and characterize a new transgenic rat model (rTg-DI) for small vessel CAA. We demonstrate that rTg-DI rats exhibit early-onset and progressive accumulation of cerebral microvascular fibrillar amyloid accompanied by behavioral deficits. Fibrils seeded from the vascular amyloid isolated from rTg-DI rats exhibit intense bands in Fourier transform infrared (FTIR) spectra characteristic of antiparallel β-sheet similar to that previously observed for human cerebral vascular amyloid [33]. Moreover, in rTg-DI rats the cerebral microvascular Aβ deposits cause

capillary structural changes, promote prominent perivascular glial activation and produce consistent, robust microhemorrhages with small vessel occlusions that are readily detected by magnetic resonance imaging.

Materials and Methods

Generation of Transgenic Rats All work with animals followed National Institutes of Health guidelines and was approved by the University of Rhode Island, Yale University and Stony Brook University Institutional Animal Care and Use Committees. A pcDNA3 vector containing 2.1 kb of human *APP* (isoform 770) cDNA was used to introduce the mutations Swedish *K670N/M671L*, Dutch *E693Q*, and Iowa *D694N* using the QuikChange kit (Stratagene, La Jolla, CA). The *APP770-SwDI* cDNA was amplified by PCR using primers containing the NheI 5-linker and SacII 3-linker. The PCR product was digested and subcloned between exons II and IV of a Thy1.2 expression cassette using NheI and SacII restriction sites. The completed construct was entirely sequenced to confirm its integrity. The 9-kb transgene was liberated by NotI/PvuI digestion, purified, and microinjected into pronuclei of Sprague-Dawley single cell embryos. Founder rats were identified by Southern blot analysis of tail DNA. Transgenic offspring were determined by PCR analysis of tail DNA using the following primers specific for human AβPP: 5'-CCTGATTGATACCAAGGAAGGCATCCTG-3' and 5'-GTCATCATCGGCTTCTTCTTCTTCCACC-3' (generating a 500-bp product). All subsequent analyses were performed with heterozygous transgenic rats.

Immunoblot Quantitation of AβPP. Rat forebrain tissues were homogenized in 10 volumes of 50 mM Tris-HCl (pH 7.5) containing 150 mM NaCl, 1% SDS, 0.5% Nonidet P-40, 5 mM EDTA, and proteinase inhibitor mixture (Roche Applied Science, Indianapolis, IN). The tissue homogenates were clarified by centrifugation at 14,000 x *g* for 10 min. Protein concentrations of the resulting supernatants were determined using the BCA protein assay Kit (Fisher Scientific, Houston, TX). The levels of AβPP in the forebrain

tissue homogenates were determined by performing quantitative immunoblotting as described [27]. Samples were probed either with monoclonal antibody P2-1, which is specific for human AβPP [34], or with monoclonal antibody 22C11 (Chemicon International, Inc., Temecula, CA), which detects both rat and human AβPP. Bands corresponding to AβPP were measured using a LICOR imaging system (Lincoln, NE).

Quantitation of Aβ Peptides Soluble pools of Aβ40 and Aβ42 were determined by performing specific ELISAs on carbonate extracted rat forebrain tissue and subsequently the insoluble Aβ40 and Aβ42 levels were determined by ELISA of guanidine lysates of the insoluble pellets resulting from the carbonate extracted rat brain tissue as described [35,36]. In the sandwich ELISAs Aβ40 and Aβ42 were captured using their respective carboxyl-terminal specific antibodies mAb2G3 and mAb21F12 and biotinylated m3D6, specific for human Aβ, was used for detection [35]. Cerebral microvessels were isolated from rat forebrains as described [27,37]. The levels of cerebral microvascular Aβ40 and Aβ42 levels were measured in guanidine lysates of the brain microvessels isolated from rTg-DI rats. Each rat brain or microvessel lysate was measured in triplicate and compared to linear standard curves generated with known concentrations of human Aβ using a Spectramax M2 plate reader (Molecular Devices, Sunnyvale, CA).

Isolation of cerebral capillary amyloid seeds. Brain capillaries were isolated from the cortices of twelve months old rTg-DI rats as described [27,37]. The isolated microvessels were analyzed microscopically by staining with thioflavin S and immunolabeling with an antibody to collagen IV to confirm the isolation of amyloid-containing microvessels. The

remaining microvessels were treated with 3 mg/ml collagenase at 37 ^{o}C overnight. The collagenase treated samples were centrifuged at 16,000 x *g* for 5 min and the resulting pellet was washed twice with TBS. The amyloid pellet was resuspended in TBS and again analyzed microscopically by staining with thioflavin S and immunolabeling with an antibody to collagen IV to confirm the isolation of vascular amyloid deposits and the absence of microvessels.

Seeding of fibrils from vascular amyloid. For the preparation of fibrils from isolated vascular amyloid, isolated vascular amyloid was sonicated for using a Fisher Scientific tip sonicator at 30% power in four 10 sec bursts. Monomeric (synthetic) Aβ40-WT peptide was added to the seeds in 3 steps at 1 h intervals. The Aβ40-WT peptide was synthesized using N-t-Boc chemistry on an ABI 430A solid-phase peptide synthesizer (ERI Amyloid Laboratory, Oxford, CT) and purified by high performance liquid chromatography (HPLC). Based on analytical reverse phase HPLC, the peptide purity was greater than 98%. The mass of the purified peptide was measured using matrix-assisted laser desorption or electrospray ionization mass spectrometry and was consistent with the calculated mass for the peptide. The peptides were isotopically labeled with 1-^{13}C at Leu17, Ala21, Gly33 and Gly37 for FTIR measurements. Purified, lyophilized Aβ peptides were aliquoted in hexafluoroisopropanol and freeze-dried for at least 4 days with a vacuum of 25 mTorr. For preparing monomeric Aβ, the peptide was dissolved in 50 mM NaOH at a concentration of 2.2 mM, then diluted in 10 mM phosphate buffer (pH 7.4) at low temperature (4 °C). The Aβ solutions were then filtered with a 0.2-micron cellulose acetate

filter to remove insoluble aggregates. The Aβ concentration was determined by the absorption at 270 nm using a molar extinction coefficient of ε=1405 $cm^{-1} \cdot M^{-1}$.

Fluorescence spectroscopy. Thioflavin T fluorescence measurements were performed on a SpectraMax M2 spectrofluorimeter plate reader. The Aβ peptide concentration was 100 μM and the thioflavin T concentration was 50 μM. Thioflavin T fluorescence was monitored every 15 sec with excitation, emission and automatic cutoff wavelengths of 446, 490 and 475 nm, respectively.

FTIR spectroscopy. FTIR spectra were obtained on a Bruker Vertex 70 spectrometer using a germanium attenuated total reflection (ATR) plate with a spectral resolution of 4 cm^{-1}. Samples were prepared by drying a 50-100 μl of peptide solution on the plate surface.

Tissue Preparation. Rats were euthanized at designated time points and perfused with cold-PBS, forebrains were removed and dissected through the mid-sagittal plane. One hemisphere was either immersion-fixed with 70% ethanol overnight and subjected to increasing sequential dehydration in ethanol, followed by xylene treatment and embedding in paraffin. Alternatively, brains were fixed with 4% paraformaldehyde overnight at 4°C and subjected to increasing concentrations (10, 20, 30%) of sucrose in PBS, then embedded in OCT compound (Sakura Finetek Inc., Torrance, CA) and snap-frozen in dry ice. Sagittal sections were cut at 10 μm thickness using a Leica RM2135 microtome (Leica Microsystems Inc., Bannockburn, IL), placed in a flotation water bath at

40°C, and then mounted on Colorfrost/Plus slides (Fisher Scientific, Houston, TX). In some cases, coronal sections were cut at 20 μm thickness from frozen brains using a Leica CM1900 cryostat (Leica Microsystems Inc.), stored in PBS with 0.02% sodium azide at 4ºC.

Immunohistochemical Analysis Antigen retrieval was performed by treating the tissue sections with proteinase K (0.2 mg/ml) for 10 min at 22 °C. Primary antibodies were detected with Alexa Fluor 594-conjugated donkey anti-rabbit or Alexa Fluor 488-conjugated goat anti-mouse secondary antibodies (1:1000). Staining for fibrillar amyloid was performed either using Amylo-Glo as described by the manufacturer (Biosensis Inc., Thebarton, South Australia) or using thioflavin S. The following antibodies were used for immunohistochemical analysis: mAb66.1 (1:250), which recognizes residues 1-5 of human Aβ [38]; mAb2B4 to detect Aβ42 (1:1000) and rabbit polyclonal antibody to detect Aβ40 (1:200; Biosource, Camarillo, CA) Aβ42, respectively; rabbit polyclonal antibody to collagen type IV to visualize cerebral microvessels (1:100; ThermoFisher, Rockford, IL); and rabbit polyclonal antibodies to GFAP (1:200; Dako, Santa Clara, CA) and Iba-1 (1:200; Fujifilm Wako Pure Chemical, Osaka, Japan) for detection of astrocytes and microglia, respectively. Prussian blue iron staining was performed to detect hemosiderin deposits reflecting signs of previous microhemorrhage [39,40]. Von Kossa calcium staining was used to detect small vessel occlusion/calcifications in the brain [41]. In this case, tissue sections were counterstained with pararosanline.

Quantitative Analysis of Vascular Pathologies The percent area amyloid coverage of cerebral microvessels, percent area iron staining and the numbers of occluded/calcified

vessels in the frontotemporal cortex, thalamic, and hippocampal regions was determined in rats at each of the specified ages using stereological principles as described [42]. Cerebral microvessel tortuosity in different brain regions was determined by immunolabeling the vessels in brain tissue sections, measuring both the traced actual vessel length and the direct straight line, end to end vessel length and dividing the actual length/direct length.

Novel Exploration Behavioral Task A novel exploration paradigm was included to measure perceptual slowing as represented in a slowed rate of stimulus encounters. This was a common deficit observed in the similar Tg-SwDI mouse model [31]. Typically, animals were placed in the open field apparatus to explore four novel and distinct objects for a 5-min trial period. Interaction with an object was scored by the AnyMaze^{tm} software as entering into a predetermined zone surrounding the object.

Magnetic Resonance Imaging Analysis All rats were deeply anesthetized with ketamine/xylazine (75 mg/kg / 10 mg/kg) i.p. followed by trans-cardial perfusion fixation. First, vascular perfusion was conducted with 0.1% heparin/PBS (20cc/min for 5 min); followed by 5% Magnevist in 10% buffered formalin solution (120 ml/rat at 20cc/min) using a Pharmacia LKB P-1 peristaltic pump. Following perfusion fixation of the 12 months old male rTg-DI and wild-type rats, the brains were removed from the skull with great care so as to not damage the brain parenchyma. The brain specimens were immersed in PBS for ≥ 4 days. All MRI acquisitions were performed on a Bruker 9.4T/30 magnet (Bruker BioSpin, Billerica MA) with BGA-12SHP imaging gradient system interfaced to an Avance III console controlled by Paravision 5.1 software. For the post-mortem high resolution

scanning we used a cryogenically cooled RF coil as a transmit and receive. The brain specimens were imbedded in fomblin (HT230-7K, Fluids & Greases, Kurt J. Lesker, Jefferson Hills, PA) and underwent MRI using a 3D gradient echo sequence with the following imaging parameters: TR/TE/FA=100ms/7~30ms/25° NEX=1 resolution= 0.08x0.08x0.08mm. The brain specimens were subsequently processed and stained for hemosiderin deposits as described above. The stained whole brain slices were digitized using an optical microscope (All-in-One Fluorescence Microscope BZ-X700), allowing the entire brain slice to be used for matching with the corresponding high-resolution post-mortem MRIs. The optical resolution achieved on the digitized brain slices was 0.377 µm/pixel.

The MRIs were displayed as isotropic 3D volumes using Amira software (Version 6.2). 3D MRIs acquired with a TE of 7ms and 18ms were used for the matching process. The process to match the MRIs to the corresponding histological brain slice involved several computational steps; and in all processing the histological brain slice served as the master template or ‘reference’ and the 3D MRI was manipulated to match it. First, 3-5 histological slices of interest were chosen which included thalamic iron staining-positive areas of micro-hemorrhages. Using the ‘slice’ feature in Amira, the MRI slice plane that best matched the histological slice - (based on anatomical landmarks such as the shape of the hippocampus, the corpus callosum, the fimbria and the shape of the ventral surface) were defined. Using rigid matching (scaling in x- and y-directions) the MRI was matched to the histological slice. Finally, the histological slice was overlaid onto the matched 2D MRI to determine the MRI signatures associated with the iron stain-positive areas.

Statistical Analysis Histological and biochemical data were analyzed by *t*-test at the 0.05 significance level. Behavioral testing data were analyzed by *t*-tests and the performance of each subject for each testing day was the average latency of the two trials.

Results

Low Level Expression of Human CAA Mutant AβPP in Brain Results in Progressive and Extensive Microvascular CAA

To target production of human chimeric Dutch/Iowa CAA mutant in neurons of rat brain we took a similar approach that was successfully used in the previous generation of our Tg-SwDI mouse line [27]. We used the neuronal-specific Thy1.2 expression cassette to drive expression human *APP* harboring the familial AD Swedish *K670N/M671L* mutations and the familial CAA Dutch *E693Q* and Iowa *D694N* mutations in neurons in the rat brain. The Swedish AβPP mutations were included solely to enhance β-secretase processing and production of Aβ peptides [43]. The familial CAA Dutch and Iowa mutations were included in the transgene to yield chimeric Dutch/Iowa CAA mutant Aβ peptides in brain which exhibit markedly enhanced fibrillogenic and vascular pathogenic properties [44,45]. The transgenic rats (rTg-DI) were generated by microinjection of the human *APP770-SwDI* construct into oocytes in a pure Sprague-Dawley background. The presence of the human AβPP transgene was confirmed in founder and subsequent

offspring rats by PCR analysis. All rTg-DI rats used in the subsequent characterization experiments were heterozygous for the human AβPP transgene.

Two months old rTg-DI rats were evaluated for expression of the human AβPP transgene using the human AβPP-specific monoclonal antibody P2-1 [34]. Immunohistochemical analysis presented in Figure 1A-F shows that human AβPP expression was evident throughout the cortex, hippocampus and thalamus and was restricted to neurons. Immunoblot analysis using mAbP2-1 confirmed that human AβPP transgene expression was only observed in rTg-DI rats (Figure 1G). Subsequent quantitative immunoblot analysis using the total (rat + human) AβPP-specific mAb22C11 showed that human transgene AβPP expression was modest and only about 50% higher than the levels of endogenous rat AβPP seen in wild-type rats (Figure 1H).

The accumulation of human Aβ peptides was measured in rTg-DI brains as they aged over 12 months. A sandwich ELISA format was used that detected only human Aβ peptides [35,36]. As the rTg-DI rats aged from 3-12 months there was a progressive increase in the amounts of soluble Aβ40 in brain whereas the amounts of soluble Aβ42 remained fairly constant over this time period (Figure 1I). The majority of soluble Aβ peptides (>90%) at each age were the shorter Aβ40 isoform. On the other hand, there was a progressive accumulation of both insoluble Aβ40 and Aβ42 as the rats aged (Figure 1J). Again, the vast majority of accumulated insoluble Aβ peptide was the shorter Aβ40 isoform. These findings indicate that despite the low level of transgene human AβPP expression there is an early-onset and progressive accumulation of Dutch/Iowa CAA mutant Aβ peptides in the brains of rTg-DI rats.

Early-Onset and Extensive Accumulation of Cerebral Microvascular Amyloid is Associated with Behavioral Impairments and Exhibits a Characteristic Anti-Parallel Alignment.

Since insoluble levels of cerebral Aβ markedly increase with age in rTg-DI rats the compartmental distribution of fibrillar amyloid was examined over time. Figure 2 shows that as early as 3 months of age there was notable accumulation of cerebral microvascular amyloid in the cortical, hippocampal and thalamic regions of the brain. Further, as the rTg-DI rats aged to twelve months there was a dramatic increase in cerebral microvascular amyloid deposition with nearly 45% and 70% of capillaries covered in fibrillar amyloid in the thalamic and hippocampal regions, respectively (Figure 2J). Although the levels of capillary CAA were somewhat lower in the cortical areas still nearly 30% of vessel surface was covered. Importantly, Figure 2K shows that these early levels of capillary CAA in the rTg-DI rats were associated with the characteristic slowing in the manner of exploration of unique objects arrayed in an open field (i.e. the novel object exploration task) consistent with a form of perceptual slowing likely to result from cortico-thalamic and hippocampal dysfunction and present in CAA [7].

Immunohistochemical analysis revealed that the vast majority of cerebral microvascular amyloid was comprised of Aβ40 (Figure 3A-C). Further, ELISA analysis of isolated cerebral microvessels from rTg-DI rats confirmed that nearly 90% of the accumulated amyloid was composed of Aβ40 peptide (Figure 3D,E). Fibrillar microvascular amyloid seeds were isolated from rTg-DI rats (Figure 3F) and FTIR spectroscopy revealed a strong β-sheet secondary structural component characteristic of

amyloid fibrils as indicated by the prominent spectral peak at ≈1632 cm^{-1} (Figure 3G). Whereas wild-type Aβ40 peptide slowly formed fibrils, the addition of the isolated microvascular amyloid seeds promoted rapid fibril assembly of wild-type Aβ40 as assayed by thioflavin T fluorescence spectroscopy (Figure 3H). The rapid increase in fluorescence argues that the Aβ monomers are using the structural template provided by the seeds as they associate with the growing fibrils. Recently, we found that fibrils seeded from cerebral vascular amyloid exhibited intense FTIR bands characteristic of antiparallel β-strand structure [33]. Notably, the newly formed seeded wild-type Aβ40 fibrils from rTg-DI microvascular amyloid exhibit a similar anti-parallel signature as reflected by the strong FTIR spectral band at ≈1607 cm^{-1} (Figure 3I).

Accumulation of Cerebral Microvascular Amyloid in rTg-DI Rats Promotes Capillary Structural Changes and Perivascular Inflammation

The prominent accumulation of cerebral microvascular amyloid in rTg-DI rats caused pronounced structural changes to cerebral capillaries compared to similarly aged wild-type rats. These capillary changes included the appearance of numerous “string vessels”, which are remnants of capillaries with no endothelial cells [46], and prominent vessel fragmentation (Figure 4B). These structural changes were accompanied by a significant ($p < 0.001$) increase in the tortuosity of the cerebral capillaries in the affected brain regions further demonstrating the deleterious effects of vascular amyloid accumulation (Figure 4C). Additionally, there was a significant ($p < 0.001$) increase in capillary area in the thalamic region and an increased trend in the other brain regions which may reflect the increased tortuosity (Figure 4D).

We also observed that cerebral microvascular amyloid in rTg-DI rats, which engages the surrounding brain parenchyma, is associated with a strong neuroinflammatory response reflected by a robust increase of perivascular reactive astrocytes (Figure 5B) when compared to similarly aged wild-type rats devoid of microvascular amyloid (Figure 5A). Likewise, an elevated number of perivascular activated microglia are present in rTg-DI rats in areas with microvascular CAA (Figure 5D). It was also noted that the lower number of microglia present in the similarly aged wild-type rats were in the resting ramified surveillance mode with numerous extended processes (Figure 5C) whereas the elevated numbers of microglia in rTg-DI rats exhibited a bushy, activated morphology actively engaged with the fibrillar amyloid deposits on the cerebral capillaries (Figure 5D). These findings indicate that the presence of prominent cerebral microvascular amyloid in rTg-DI rats is accompanied by structural deterioration of brain capillaries and a robust increase in activated perivascular glial cells.

Robust Microhemorrhages and Small Vessel Occlusions are Detected by MRI in rTg-DI Rats

A prominent clinical feature of CAA in humans is the presence of cerebral microbleeds [1,2]. The presence of microbleeds was histochemically evaluated by Perl's staining for perivascular hemosiderin deposits in groups of progressively aged rTg-DI rats. Evidence of cerebral microbleeds was observed in the cortical and hippocampal regions of 12 months old rTg-DI rats (Figures 6A and 6B, respectively). However, microbleeds were particularly abundant in the thalamic region of the brain with various presentations of perivascular iron deposits including tightly-associated crescent shaped

deposits (Figure 6C), complete circumferential involvement (Figure 6D), indications of multiple bleeds in several adjacent microvessels (Figure 6E) and more diffuse perivascular iron deposits (Figure 6F). Since it was often difficult to discriminate between individual and grouped microbleeds we measured the area of iron deposition in the different brain regions at 6 and 12 months. As shown in Figure 6G, signs of microbleeds in the cortex were not observed at 6 months and were low at 12 months. However, in the hippocampus small areas of microbleeds were detected at 6 months and this increased as the rTg-rats aged to 12 months. Most notably, in the thalamus there was clear evidence of microbleeds at 6 months which dramatically increased at 12 months of age with >1% of the total thalamic area covered with perivascular iron deposits. Although microbleeds are numerous in 12 months old rTg-DI rats large macrobleeds have not been observed at this age.

Small vessel occlusions and calcifications are other microvasculopathies observed in CAA patients [2,47,48]. Interestingly, in the thalamic region of prevalent microbleeds in rTg-DI rats we noted numerous occluded microvessels (Figure 7A). Calcium staining of adjacent brain tissue sections indicated calcifications in these small vessel occlusions surrounded by areas of fibrinoid necrosis (Figure 7B). These microvascular occlusions were bilateral and largely restricted to the ventral posterior lateral nucleus of the thalamic region (Figure 7C). The overall numbers of these thalamic small vessel occlusions were quantified in rTg-DI rats as they aged from 3 to 12 months of age. As shown in Figure 7D, the occlusions were extremely rare or absent at 3 months of age. However, at 6 and 12 months the numbers markedly increased to ≈40 and ≈115 small vessel occlusions,

respectively in this thalamic region. At each age the majority of the vessel occlusions were in capillaries but occasionally larger microvessels were also occluded.

We next performed studies in rTg-DI rats to characterize the microhemorrhages in situ using *in vitro* MR microscopy. Figure 8 shows the results of MRI-to-histology matching from a 12 months old rTg-DI rat with documented thalamic microhemorrhages and small vessel occlusions. A 2D T2*-weighted MRI (TE=7ms) (Figure 8A) was matched to the corresponding Perl iron-stained histological slice (Figure 8B). The dense dark areas in the thalamus shown on the T2*-weighted MRI are corresponding to the microvessels identified by Perl-stained iron deposits associated with the microbleeds and occluded vessels. The Perl-stained histological slice is overlaid on the T2*-weighted images under conditions where the histological slice has been rendered transparent to highlight the low signal intensity 'susceptibility' features on the T2*-weighted MRI observed in the thalamus, bilaterally, which is caused by presence of iron. Panels 8C and 8E are high magnification of the inserts in panels 8B and 8D, respectively. Figures 8F and 8G are 3-D volume rendered MRIs of the same rat showing the brain outlined in light yellow; and the Perl-stain iron-positive associated low signal intensity area in the thalamus have been volume rendered (green) to illustrate the near-perfect bilateral symmetry of the microhemorrhages and occluded microvessels in the thalamic areas. Together, these findings indicate that rTg-DI develop numerous and consistent thalamic microhemorrhages and microvessel occlusions that are readily detected by T2*-weighted MRI.

Discussion

CAA is a common cerebral small vessel disease of the elderly and a prominent comorbidity of AD that promotes and exacerbates VCID, yet our understanding of the condition remains limited and despite the high prevalence there is no effective treatment. Several transgenic mouse models, that develop varying levels of CAA, have been in use for more than a decade and have provided better insight into the pathogenesis of CAA [23-32]. However, their usefulness to further investigate CAA from the point of view of faithfully recapitulating the human condition is limited due to their biological evolutionary distance from humans and the small size of their brains which can be problematic for effective neuroimaging *in vivo*. Further, complicated cognitive testing to investigate VCID in the setting of evolving CAA can be unreliable due to temperamental variability in mice [49]. Although naturally occurring models of CAA exist, most notably canines and non-human primates, the experimental use of these species for large cohort experimentation and testing is limited due to the cost and time needed for CAA to develop (decade or decades) [50]. Thus, there is a need for a better experimental model of CAA. The use of rats, specifically transgenic rats, to investigate the pathogenesis of human CNS disorders offers several distinct advantages over transgenic mice. First, rats are evolutionarily 4-5 million years closer to humans [51]. Thus, the genetics, physiology and brain morphology of rats are better suited to model human CAA. Second, the larger brain size and increased white-to-grey matter ratio of the rat enables structural neuroimaging studies with superior contrast- and signal-to-noise ratio compared to mice. Lastly, rats provide the opportunity

for far more sophisticated cognitive testing compared to mice thereby bridging a gap in knowledge as to how CAA drives VCID [52].

In the current study, we describe the generation and initial characterization of a novel transgenic rat model (rTg-DI) of microvascular type 1 CAA. The rTg-DI rats were designed from our earlier success in generating Tg-SwDI transgenic mice that develop early-onset and progressive cerebral microvascular amyloid deposition [27]. In the rTg-DI rats, we similarly expressed the human AβPP transgene harboring the Swedish familial AD mutations and the β-secretase cleavage site and the chimeric Dutch E693Q/Iowa D694N familial CAA mutations in neurons in the brain. Indeed, low level neuronal expression of the human AβPP transgene was observed in the rTg-DI rats (Figure 1). This phenotype is important because it signifies that our new CAA model does not require abnormal, vast over-expression of human AβPP and production of human Aβ, that is commonly found in other transgenic rodent models, which can introduce potential confounds on neuronal function. This underscores that the robust cerebral accumulation of Aβ and specific development of microvascular CAA is a consequence of the chimeric familial Dutch/Iowa mutations in the Aβ peptide that is produced in the brains of these rats. Interestingly, the early-onset development of microvascular CAA and associated neuroinflammation coincides with early-onset and sustained cognitive deficits in rTg-DI rats and offers the promise of a unique model for the future elucidation as to how CAA can promote VCID.

The type and form of amyloid that accumulates in the cerebral microvasculature of rTg-DI rats is remarkably similar to what is found in human CAA. For example, in contrast to parenchymal amyloid plaques that largely accumulate fibrillar Aβ42 in both humans

and rodent models, the fibrillar cerebral vascular amyloid deposits in rTg-DI rats are composed primarily of the shorter Aβ40 species [53,54]. In addition to the difference in the length of the Aβ peptide that forms the amyloid fibrils in either parenchymal plaques or cerebral vascular deposits other micro-structural differences have been found. Recently, we found that fibrils produced from seeds of cerebral vascular fibrillar amyloid deposits exhibit increased intensity in FTIR spectra that is characteristic of anti-parallel structure of the β strands forming the backbone of the Aβ fibrils [33]. This structure is distinct from the parallel registry observed in parenchymal plaque amyloid fibrils [55,56]. The β-sheet, anti-parallel fibril character is also observed in the cerebral microvascular amyloid deposits of the rTg-DI rats (Figure 3). This important distinction between parenchymal and cerebral vascular amyloid fibrils likely is involved in the pathogenesis of these two types of deposits and may have important consequences with regards to subsequent pathologies associated with each lesion type.

The accumulation of cerebral microvascular amyloid in rTg-DI rats promotes distinct vessel and perivascular changes that are reflected in human CAA. Structurally, the accumulation of microvascular amyloid causes significant alterations in capillary morphology including increased vessel fragmentation, occlusion and tortuosity (Figure. 4). It has been suggested that these types of structural alterations can impair capillary blood flow and may cause hypertension upstream from these sites of disruption [57]. On the other hand, capillary tortuosity caused by microvascular amyloid can lead to poor perfusion and downstream infarction [22,58]. Interestingly, there was an increase the capillary area in the thalamic region of rTg-DI rats which might reflect the measured increase in capillary tortuosity. Alternatively, it is possible that there is an increase in

vascularization in response to the extensive amyloid-mediated damage to the microvasculature in this region. The changes in capillary morphology likely contribute to increased perivascular disturbances in fluid homeostasis, inflammation, thrombosis and microhemorrhage observed in CAA. In line with this, the accumulation of fibrillar amyloid along the capillaries of rTg-DI rats induces a strong neuroinflammatory response characterized by activation and robust increases in perivascular astrocytes and microglia which is accompanied by consistent and frequent microbleeds and microvascular occlusions, particularly in the thalamic region. These latter thrombotic events may result directly from the excessive amyloid deposition in this region but are more likely to be related to downstream inflammatory responses triggered by amyloid accumulation.

Currently, outside of biopsy or autopsy confirmation, the clinical diagnosis of CAA is based on the “Boston criteria” which relies primarily on the detection of lobar microbleeds based on MR imaging hypointensities resulting from perivascular hemosiderin [3,59]. Similarly, MR imaging analysis of rTg-DI rats readily detected the perivascular hemosiderin associated with the prevalent thalamic microbleeds. 3-D reconstruction of the MR defined hypointensities illustrated the symmetrical and bilateral nature of these consistent thalamic microbleeds (Figure 8). These findings suggest that similar parameters for the “Boston criteria” diagnosis of CAA in humans can be applied to rTg-DI rats allowing for the opportunity to investigate the longitudinal development and persistence of these hallmark lesions by clinical relevant methodology.

Although the extent of CAA, capillary structural changes and perivascular neuroinflammation is high in several brain regions of rTg-DI rats at six to twelve months it is currently unclear why the most severe associated events of microhemorrhage and

vessel occlusion are largely restricted bilaterally to the thalamic regions. In human CAA, cerebral microbleeds tend to be found in lobar cortical regions, in particular the occipital cortex, and not so frequently in deeper brain structures. However, in cerebral autosomal dominant arteriopathy with subcortical infarcts and leukoencephalopathy (CADASIL), another type of cerebral small vessel disease, thalamic microbleeds are commonly observed both in humans and in the equivalent transgenic mouse model [60-62]. Perhaps the thalamic region in rats exhibits differential blood flow or perivascular clearance mechanisms compared to humans and in other regions of the rat brain making this region particularly susceptible to excessive perivascular amyloid deposition. Alternatively, rat capillaries/microvessels in the thalamic areas may possess a different vascular environment compared to other brain regions. Future studies are needed to evaluate these possibilities. Although the anatomical distribution of CAA and cerebral vascular thrombotic lesions may be somewhat different between rTg-DI rats and humans this unique model provides new opportunities to investigate the pathogenic development of CAA and its relation of VCID. Further, rTg-DI rats provide an improved platform for the development of biomarkers and preclinical testing of therapeutic interventions for this common small vessel disease.

Acknowledgements

Antibody reagents for the Aβ ELISA were generously provided by Lilly Research Laboratories, Indianapolis, IN.

References

1. Banerjee G, Carare, R, Cordonnier C, Greenberg SM, Schneider JA, Smith EE, Buchem MV, Grond JV, Verbeek MM, Werring DJ: The increasing impact of cerebral amyloid angiopathy: essential new insights for clinical practice. J Neurol Neurosurg Psychiatry 2017, 88:982-994

2. Auriel E, Greenberg SM: The pathophysiology and clinical presentation of cerebral amyloid angiopathy. Curr Atheroscler Rep 2012, 14:343-350

3. Biffi A, Greenberg SM: Cerebral amyloid angiopathy: a systematic review. J Clin Neurol 2011, 7:1-9

4. Greenberg SM, Gurol ME, Rosand J, Smith EE: Amyloid angiopathy-related vascular cognitive impairment. Stroke 2004, 35:2616-2619

5. Attems J, Jellinger K, Thal DR, Van Nostrand W: Review: sporadic cerebral amyloid angiopathy. Neuropathol Appl Neurobiol 2011, 37:75-93

6. Thal DR, Ghebremedhin E, Rub U, Yamaguchi H, Del Tredici K, Braak H: Two types of sporadic cerebral amyloid angiopathy. J Neuropath Exper Neurol 2002, 61:282-293

7. Arvanitakis Z, Leurgans SE, Wang Z, Wilson RS, Bennett DA, Schneider J: Cerebral amyloid angiopathy pathology and cognitive domains in older persons. Ann Neurol 2011, 69:320-327

8. Boyle PA, Yu L, Nag S, Leurgans S, Wilson RS, Bennett DA, Schneider J: Cerebral amyloid angiopathy and cognitive outcomes in community-based older persons. Neurology 2015, 85:1930-1936

9. Jellinger KA: Alzheimer disease and cerebrovascular pathology: an update. J Neural Transm 2002, 109:813-836

10. Launer LJ, Petrovitch H, Ross GW, Markesbery W, White LR: AD brain pathology: vascular origins? Results from the HAAS autopsy study. Neurobiol Aging 2008, 29:1587-1590

11. Esiri M, Chance S, Joachim C, Warden D, Smallwood A, Sloan, C, Christie S, Wilcock G, Smith AD: Cerebral amyloid angiopathy, subcortical white matter disease and dementia: literature review and study in OPTIMA. Brain Pathol 2015, 25:51-62

12. Levy E, Carman M, Fernandez-Madrid, IJ, Power MD, Lieberburg I, van Duinen S, Bots GT, Luyendijk W, Frangione B: Mutation of the Alzheimer's disease amyloid gene in hereditary cerebral hemorrhage, Dutch type. Science 1990, 248:1124-1126.

13. Van Broeckhoven C, Haan J, Bakker E, Hardy JA, Van Hul W, Wehnert A, Vegter-Van der Vlis M, Roos RA: Amyloid β protein precursor gene and hereditary cerebral hemorrhage with amyloidosis (Dutch). Science 1990, 248:1120-1122.

14. Grabowski TJ, Cho HS, Vonsattel JP, Rebeck GW, Greenberg SM: Novel amyloid precursor protein mutation in an Iowa family with dementia and severe cerebral amyloid angiopathy. 2001, Ann Neurol 49:697-705

15. Rensink AA, de Waal RM, Kremer B, Verbeek MM: Pathogenesis of cerebral amyloid angiopathy. Brain Res Brain Res Rev 2003, 43:207-223

16. Eikelenboom P, Veerhuis R, Familian A, Hoozemans JJ, van Gool WA, Rozemuller AJM: Neuroinflammation in plaques and vascular β-amyloid disorders: Clinical and therapeutic implications. Neurodegener Dis 2008, 5:190-193

17. Richard E, Carrano A, Hoozemans JJ, van Horssen J, van Haastert ES, Eurelings LS, de Vries HE, Thal DR, Eikelenboom P, van Gool WA, Rozemuller AJ: Characteristics of dyshoric capillary cerebral amyloid angiopathy. J Neuropathol Exp Neurol 2010, 69:1158-1167

18. Thal DR, Ghebremedhin E, Orantes M, Wiestler OD: Vascular pathology in Alzheimer's disease: Correlation of cerebral amyloid angiopathy and arteriosclerosis/lipohyalinosis with cognitive decline. J Neuropath Exp Neurol 2003, 62:1287-1301

19. Attems J, Jellinger KA: Only cerebral capillary amyloid angiopathy correlates with Alzheimer pathology—a pilot study. Acta Neuropathol 2004, 107:83-90

20. Bailey TL, Rivara CB, Rocher AB, Hof PR: The nature and effects of cortical microvascular pathology in aging and Alzheimer's disease. Neurol Res 2004, 26:573-578

21. Rozemuller AJ, van Gool WA, Eikelenboom P: The neuroinflammatory response in plaques and amyloid angiopathy in Alzheimer's disease: therapeutic implications. Curr Drug Targets CNS Neurol Disord 2005, 4:223-233

22. Hecht M, Kramer LM, von Arnim CAF, Otto M, Thal DR: Capillary cerebral amyloid angiopathy in Alzheimer's disease: association with allocortical/hippocampal microinfarcts and cognitive decline. Acta Neuropathol 2018, 135:681-694

23. Games D, Adams D, Alessandrini R, Barbour R, Berthelette P, Blackwell C, Carr T, Clemens J, Donaldson T, Gillespie F, Guido T, Hagopian S, Johnson-Wood K, Khan K, Lee M, Leibowitz P, Lieberberg I, Little S, Masliah E, McConlogue L, Montoya-Zavala M, Mucke L, Paganini L, Penniman E, Power M, Schenk D, Seubert P, Snyder B, Soriano F, Tan H, Vitale J, Wadsworth S, Wolozin B, Zhao J: Alzheimer-type neuropathology in transgenic mice overexpressing V717F β-amyloid precursor protein. Nature 1995, 373:523-527

24. Hsiao K, Chapman P, Nilsen S, Eckman C, Harigaya Y, Younkin S, Yang F, Cole G: Correlative memory deficits, Aβ elevation, and amyloid plaques in transgenic mice. Science 1996, 274:99-102

25. Calhoun ME, Burgermeister P, Phinney AL, Stalder M, Tolnay M, Wiederhold K-H, Abramowski D, Sturchler-Pierrat C, Sommer B, Staufenbiel M, Jucker M: Neuronal overexpression of mutant amyloid precursor protein results in prominent deposition of cerebrovascular amyloid. Proc Natl Acad Sci USA 1999, 96:14088-14093

26. Oakley H, Cole SL, Logan S, Maus E, Shao P, Craft J, Guillozet-Bongaarts A, Ohno M, Disterhoft J, Van Eldik L, Berry R, Vassar R: (2006) Intraneuronal ß-amyloid aggregates, neurodegeneration, and neuron loss in transgenic mice with five familial Alzheimer's disease mutations: potential factors in amyloid plaque formation. J Neurosci 2006, 26:10129-10140

27. Davis J, Xu F, Deane R, Romanov G, Previti ML, Zeigler K, Zlokovic BV, Van Nostrand WE: Early-onset and robust cerebral microvascular accumulation of amyloid β-protein in transgenic mice expressing low levels of a vasculotropic Dutch/Iowa mutant form of amyloid β-protein precursor. J Biol Chem 2004, 279:20296-20306

28. Herzig MC, Winkler DT, Burgermeister P, Pfeifer M, Kohler E, Schmidt SD, Danner S, Abramowski D, Sturchler-Pierrat C, Buki K, van Duinen SG, Maat-Schieman MLC, Staufenbiel M, Matthews PM, Jucker M: Aβ is targeted to the vasculature in a mouse model of hereditary cerebral hemorrhage with amyloidosis. Nature Neurosci 2004, 7:954-960

29. Miao J, Xu F, Davis J, Otte-Holler I, Verbeek MM, Van Nostrand WE: Cerebral microvascular amyloid β protein deposition induces vascular degeneration and neuroinflammation in transgenic mice expressing human vasculotropic mutant amyloid β precursor protein. Am J Pathol 2005, 167:505-515

30. Miao J, Vitek MP, Xu F, Previti ML, Davis J, Van Nostrand WE: Reducing cerebral microvascular amyloid β protein deposition diminishes regional neuroinflammation in vasculotropic mutant amyloid precursor protein transgenic mice. J Neurosci 2005, 25:6271-6277

31. Xu F, Grande AM, Robinson JK, Previti ML, Davis J, Van Nostrand WE: Early-onset subicular microvascular amyloid and neuroinflammation correlate with behavioral deficits in vasculotropic mutant AβPP transgenic mice. Neuroscience 2007, 146:98-107

32. Xu W, Xu F, Anderson ME, Kotarba AE, Davis J, Robinson JK, Van Nostrand WE: Cerebral microvascular rather than parenchymal amyloid β-protein pathology promotes early cognitive impairment in transgenic mice. J Alzheimers Dis 2014, 38:621-632

33. Xu F, Fu Z, Dass S, Kotarba AE, Davis J, Smith SO, Van Nostrand WE: Cerebral vascular amyloid seeds drive amyloid β-protein fibril assembly with a distinct anti-parallel structure. Nature Comm 2016, 7:13527

34. Van Nostrand WE, Wagner SL, Suzuki M, Choi BH, Farrow JS, Geddes JW, Cotman CW, Cunningham DD: Protease nexin-II, a potent anti-chymotrypsin, shows identity to amyloid b-protein precursor. Nature 1989, 341:546-549

35. Johnson-Wood K, Lee M, Motter R, Hu K, Gordon G, Barbour R, Khan K, Gordon M, Tan H, Games D, Lieberburg I, Schenk D, Seubert P, McConlogue L: Amyloid precursor protein processing and Aβ42 deposition in a transgenic mouse model of Alzheimer's disease. Proc Natl Acad Sci USA 1997, 94:1550-1555

36. DeMattos RB, O'dell M, Parsadanian M, Taylor JW, Harmony JA, Bales KR, Paul SM, Aronow BJ, Holtzman DM: (2002) Clusterin promotes amyloid plaque formation and is critical for neuritic toxicity in a mouse model of Alzheimer's disease. Proc Natl Acad Sci USA 2002, 99:10843-10848

37. Zlokovic BV, Mackic JB, Wang L, McComb JG, McDonough A: Differential expression of Na,K-ATPase alpha and beta subunit isoforms at the blood-brain barrier and the choroid plexus. J Biol Chem 1993, 268:8019-8025

38. Deane R, Yan SD, Submamaryan RK, LaRue B, Jovanovic S, Hogg E, Welch D, Manness L, Lin C, Yu J, Zhu H, Ghiso J, Frangione B, Stern A, Schmidt AM, Armstrong DL, Arnold B, Liliensiek B, Nawroth P, Hofman F, Kindy M, Stern D, Zlokovic B: RAGE mediates amyloid beta-peptide transport across the blood-brain barrier and accumulation in brain. Nature Med 2003, 9:907-913

39. Gomori G: Microtechnical demonstration of iron. Am J Pathol 1936, 12:655-663

40. Winkler DT, Bondolfi L, Herzig MC, Jann L, Calhoun ME, Weiderhold KH, Tolnay M, Staufenbiel M, Jucker M: Spontaneous hemorrhagic stroke in a mouse model of cerebral amyloid angiopathy, J Neurosci 2001, 21:1619-1627

41. Rungby J, Kassem M, Fink Eriksen E, Danscher G: The von Kossa reaction for calcium deposits: silver lactate staining increases sensitivity and reduces background. Histochem J 1993, 25:446-451

42. Long JM, Kalehua AN, Muth NJ, Hengemihle JM, Jucker M, Calhoun ME, Ingram DK Mouton PR: Stereological estimation of total microglia number in mouse hippocampus. J Neurosci Methods 1998, 84:101-108

43. Mullan M, Crawford F, Axelman K, Houlden H, Lilius L, Winblad B, Lannfelt L: A pathogenic mutation for probable Alzheimer's disease in the APP gene at the N-terminus of beta-amyloid. Nature Genetics 1992, 1:345-347

44. Davis J, Van Nostrand WE: (1996) Enhanced pathologic properties of Dutch-type mutant amyloid β-protein. Proc Natl Acad Sci USA 1996, 93:2996-3000

45. Van Nostrand WE, Melchor JP, Cho HS, Greenberg SM, Rebeck GW: Pathogenic effects of D23N Iowa mutant amyloid β-protein. J Biol Chem 2001, 276:32860-32866

46. Brown WR: A review of string vessels or collapsed, empty basement membrane tubes. J Alzheimers Dis 2010, 21:725-739

47. Vinters HV, Natte R, Maat-Schieman ML, van Duinen SG, Hegeman-Kleinn I, Welling-Graafland C, Haan J, Roos RA: Secondary microvascular degeneration in amyloid angiopathy of patients with hereditary cerebral hemorrhage with amyloidosis, Dutch type (HCHWA-D). Acta Neuropathol 1998, 95:235-244

48. Sellal F, Wallon D, Martinez-Almoyna L, Marelli C, Dhar A, Oesterle H, Rovelet-Lecrux A, Rousseau S, Kourkoulis CE, Rosand J, DiPucchio ZY, Frosch M, Gombert C, Audoin B, Mine M, Riant F, Frebourg T, Hannequin D, Campoin D, Greenberg SM, Tournier-Lasserve E, Nicolas G: APP mutations in cerebral amyloid angiopathy with or without cortical calcifications: Report of three families a literature review. J Alzheimers Dis 2017, 56:37-46

49. Bailey KR, Rustay NR, Crawley JN: Behavioral phenotyping of transgenic and knockout mice: practical concerns and potential pitfalls. ILAR J 2006, 47:124-131

50. Jakel L, Van Nostrand WE, Nicoll JAR, Werring DJ, Verbeek MM: Animal models of cerebral amyloid angiopathy. Clin Sci 2017, 131:2469-2488

51. Yang S, Smit AF, Schwartz S, Chiaromonte F, Roskin KM, Haussler D, Miller W, Hardison RC: Patterns of insertions and their covariation with substitutions in the rat, mouse, and human genomes. Genome Res 2004, 14:517-527

52. Ellenbroek B, Youn J: Rodent models in neuroscience research: is it a rat race? Disease Models & Mechanisms 2016, 9:1079-1087

53. Miller DL, Papayannopoulos IA, Styles J, Bobin SA, Lin YY, Biemann K, Iqbal K: Peptide composition of the cerebrovascular and senile plaque core amyloid deposits of Alzheimer’s disease. Arch Biochem Biophys 1993, 301:41-52

54. Alonzo NC, Hyman BT, Rebeck GW, Greenberg SM: Progression of cerebral amyloid angiopathy: accumulation of amyloid-beta40 in affected vessels. J Neuropathol Exp Neurol 1998, 57:353-359

55. Paravastua AK, Leapman RD, Yau WM, Tycko R: Molecular structural basis for polymorphism in Alzheimer's β-amyloid fibril. Proc Natl Acad Sci USA 2008, 105:18349-18354

56. Tycko R: Solid-State NMR sudies of amyloid fibril structure. Ann Rev Phys Chem 2011, 62, 279-299

57. Moody DM, Brown WR, Challa VR, Ghazi-Birry HS, Reboussin DM: Cerebral microvascular alterations in aging, leukoaraiosis, and Alzheimer’s disease. Ann NY Acad Sci 1997, 826:103-116

58. Brown WR, Moody DM, Thore CR, Anstrom JA, Challa VR: Microvascular changes in the white matter in dementia. J Neurol Sci 2009, 283:28-31

59. Greenberg SM, Charidimou A: Diagnosis of cerebral amyloid angiopathy: Evolution of the Boston Criteria. Stroke 2018, 49:491-497

60. Lesnik Oberstein SA, van dem Boom R, van Buchem MA, van Houwelingen HC, Bakker E, Vollebregt E, Ferrari MD, Breuning MH, Hann J, Dutch CADASIL Research Group: Cerebral microbleeds in CADASIL. Neurology 2001, 57:1066-1070

61. Lee JS, Kang CH, Park SQ, Choi HA, Sim KB: Clinical significance of cerebral microbleeds locations in CADASIL with R544C NOTCH3 mutation. PLOS one 2015, 10:e0125297

62. Wallays G, Nuyens D, Silasi-Mansat R, Souffreau J, Callaerts-Vegh Z, Van Nuffelen A, Moons L, D’Hooge R, Lupu F, Carmeliet P, Collen D, Dewerchin M: Notch3 Arg170Cys knock-in mice display pathologic and clinical features of the neurovascular disorder cerebral autosomal dominant arteriopathy with subcortical infarcts and leukoencephalopathy. Arterioscler Thromb Vasc Biol 2011, 31:2881-2888

Figure Legends

Figure 1. Analysis of transgenic human AβPP expression and progressive Aβ accumulation in rTg-DI rats.

Brain sections from two months old rTg-DI rats were immunolabeled with the mouse monoclonal antibody mAbP2-1 to specifically detect human AβPP (green) and the rabbit polyclonal antibody NeuN to detect neurons (red). There was widespread human AβPP expression in neurons in the cortex (**A,B**), hippocampus (**B,D**) and thalamus (**E,F**). Scale bars = 10 µm (**A,C,E**) and 50 µm (**B,D,F**). (**G**) Immunoblot analysis of human AβPP expression in total brain homogenates from wild-type rats and rTg-DI rats. (**H**) Quantitative immunoblotting was performed to measure total AβPP (endogenous rat AβPP + transgenic human AβPP) in brain homogenates of wild-type rats and rTg-DI rats. The data presented are the means ± S.D. of 5 rats per each group (*$p < 0.05$). The level of transgene human AβPP expression is ≈50% the amount of endogenous rat AβPP. The levels of soluble (**I**) and insoluble (**J**) Aβ40 and Aβ42 peptides in the forebrain of progressively aged rats were measured by ELISA as described under "Experimental Procedures." The data presented are the means ± S.D. of triplicate measurements in 5-6 rTg-DI rats per group.

Figure 2. Progressive Accumulation of Microvascular CAA in rTg-DI Rats.

Brain sections from rTg-DI rats at three months old (**A-C**), six months old (**D-F**) and twelve months old (**G-I**) were stained for fibrillar amyloid using thioflavin-S (green) and immunolabeled for collagen type IV to identify cerebral microvessels (red). Scale bars =

50 μM. The rTg-DI rats develop early-onset and progressive cerebral microvascular fibrillar amyloid in the cortical, hippocampal and thalamic regions. (**J**) Quantitation of microvascular thioflavin-S positive amyloid load in different brain regions of three months (blue bars), six months (gray bars) and twelve months (red bars) old rTg-DI rats. Data shown are mean ± S.D of 6-7 rTg-DI rats per group. (**K**) rTg-DI rats showed consistently fewer return approaches within a session to four novel objects placed in an open field arena compared to WT rats at 3 and 12 months of age (*$p < 0.05$).

Figure 3. Analysis of Cerebral Microvascular Aβ Deposition in rTg-DI Rats.

Brain sections from rTg-DI rats at twelve months of age were immunolabeled with an antibody specific for Aβ40 (red) (**A**) and an antibody specific for Aβ42 (green) (**B**) and merged (**C**). Scale bar = 50 μm. (**D**) Cerebral microvessels were isolated from twelve months old rTg-DI rats and stained with thioflavin-S to visualize fibrillar amyloid deposits (green) and immunolabeled with an antibody to collagen IV to view the cerebral microvessels (red). Scale bar = 50 μm. (**E**) ELISA measurements were performed to determine the amounts of Aβ40 and Aβ42 in the microvessels isolated from rTg-DI rat brain. Data shown are mean ± S.D. of 5 rTg-DI rats. (**F**) Cerebral microvascular amyloid deposits after digestion and removal of the capillaries and stained for fibrillar amyloid using thioflavin S (green). Scale bar = 50 μm. (**G**) FTIR spectra in the region of the amide I vibration of vascular amyloid isolated from vessels of rTg-DI rat brain. (**H**) Thioflavin T fluorescence of fibril formation from seeds obtained from isolated vascular amyloid. Thioflavin fluorescence increases rapidly upon the addition of 100 μM Aβ40-WT monomer to sonicated vascular amyloid (black). Monomeric Aβ40-WT peptide exhibits a much

slower increase in fluorescence in the absence of fibril seeds (blue). (**I**) FTIR spectra in the region of the amide I vibration of Aβ40-WT fibrils produced from seeds of the rat vascular amyloid. The amide I vibration at 1632 cm^{-1} corresponds to β-sheet. The vibration at 1607 cm^{-1} corresponds to the amide vibration shifted as a result of $^{13}C=O$ labels at the backbone carbonyls of Leu17, Ala21, Gly33 and Gly37. The large intensity of the 1607 cm^{-1} band relative to the β-sheet vibration at 1632 cm^{-1} is characteristic of anti-parallel β-sheet structure. The spectra were obtained after incubation for 48 h at 37 °C.

Figure 4. Cerebral Microvascular Structural Changes in rTg-DI Rats.

Brain sections from wild-type rats (**A**) and rTg-DI rats (**B**) at twelve months of age were immunolabeled with an antibody to collagen IV to identify cerebral microvessels. Images shown are from the thalamic region of the rats. Numerous fragmented and string vessels (white arrows) were identified in the rTg-DI rats. Scale bars = 50 μm. (**C**) The tortuosity of the cerebral capillaries was measured in the cortex, hippocampus and thalamic region of wild-type and rTg-DI. Data shown are mean ± S.D. of 5-6 rats per group (***$p < 0.001$). (**D**) The capillary area was measured in the cortex, hippocampus and thalamic region of wild-type and rTg-DI. Data shown are mean ± S.D. of 5-6 rats per group (***$p < 0.001$). The data show that cerebral capillaries in rTg-DI rats exhibit structural abnormalities, increased tortuosity and, in the thalamic region, increased vascularization.

Figure 5. Perivascular Glial Activation in rTg-DI Rats.

Twelve months old brain sections from wild-type rats (**A,C**) and rTg-DI rats (**B,D**) were stained for fibrillar amyloid (blue), immunolabeled with an antibody to collagen IV to identify cerebral microvessels (red) and immunolabeled with an antibody to GFAP to identify astrocytes (green) (**A,B**) or immunolabeled with an antibody to Iba-1 to identify microglia (green) (**C,D**). Scale bars = 50 µm. rTg-DI rats exhibit strong increases in perivascular reactive astrocytes and activated microglia in response to the prominent cerebral microvascular amyloid.

Figure 6. Prominent Cerebral Microhemorrhages in rTg-DI Rats.

Twelve months old brain sections from rTg-DI rats were stained for hemosiderin to identify microhemorrhages (blue) in the cortex (**A**), hippocampus (**B**) and the thalamus (**C-F**). Scale bars = 50 µm. The percent area fraction of hemosiderin staining was quantitated in the cortex, hippocampus and thalamus of six months old (gray) and twelve months old (red) rTg-DI rats (**G**). Data represent the mean ± S.D. of 6-7 rTg-DI rats per group. Progressive and consistent accumulation of microbleeds was observed, particularly in the thalamus, of rTg-DI rats.

Figure 7. Progressive Cerebral Microvascular Occlusions in rTg-Rats.

Twelve months old brain sections from rTg-DI rats were stained for hemosiderin to identify microhemorrhages (blue) and counterstained with pararosanline (pink) in the thalamus (**A**). Scale bar = 50 µm. Adjacent tissue sections were stained for calcium (black) and counterstained with pararosanline (pink) in the thalmus (**B**). Scale bar = 50 µm. Lower magnification revealed that the occluded, calcified microvessels were restricted to the

thalamic region (**C**). Scale bar = 200 µm. The number of thalamic microvessel occlusions were counted in progressively aged rTg-DI rats (**D**). Data represent the mean ± S.D. of 5-6 rTg-DI rats per group. Numerous occluded capillary/microvessels were observed around microbleeds specifically in the thalamic region of rTg-DI rats.

Figure 8. Detection of Microhemorrhage by MRI in rTg-DI Rats. (**A**) 2D T2*-weighted MRI (TE=7ms) matched to the corresponding Perl-stained histological slice (**B**). The dense dark areas in the thalamus shown on the T2*-weighted MRI (**A**) correspond to microvessels characterized by Perl stain-positive microbleeds and occluded vessels. (**D**) Perl-stained histological slice was overlaid on the T2*-weighted images under conditions where the histological slice have been rendered transparent to highlight the low signal intensity 'susceptibility' features on the T2*-weighted MRI observed bilaterally in the thalamus, which is caused by presence of hemosiderin. Scale bars = 500 µm. Panels **(C)** and **(E)** are higher magnification of the inserts in **(B)** and **(D)**, respectively. Scale bars = 100 µm. Panels (**F**) and (**G**) are 3D volume rendered MRIs of the same rat showing the brain outlined in light yellow; and the Perl stain-positive associated low signal intensity area in the thalamus have been volume rendered (green) to illustrate the near-perfect symmetry of the microhemorrhage/occluded microvessels areas. Scale bar = 3.5 mm.

Figure 1

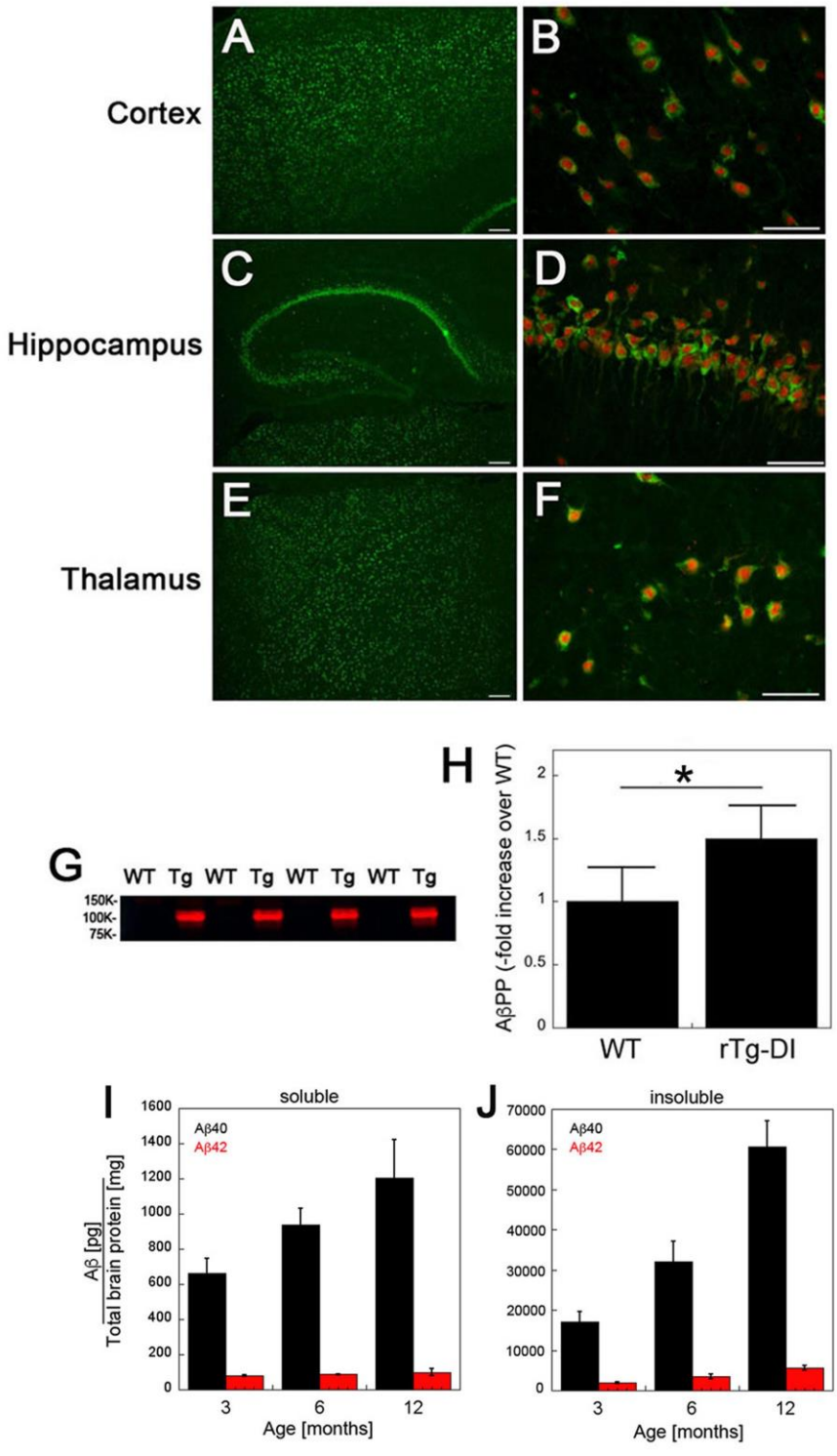
A
B
Cortex
C
D
Hippocampus
E
F
Thalamus
G
WT Tg WT Tg WT Tg WT Tg
150K-
100K-
75K-
H
AβPP (-fold increase over WT)
2
1.5
1
0.5
0
*
WT
rTg-DI
I
soluble
Aβ40
Aβ42
Aβ [pg] / Total brain protein [mg]
1600
1400
1200
1000
800
600
400
200
0
3
6
12
Age [months]
J
insoluble
Aβ40
Aβ42
70000
60000
50000
40000
30000
20000
10000
0
3
6
12
Age [months]

Figure 2

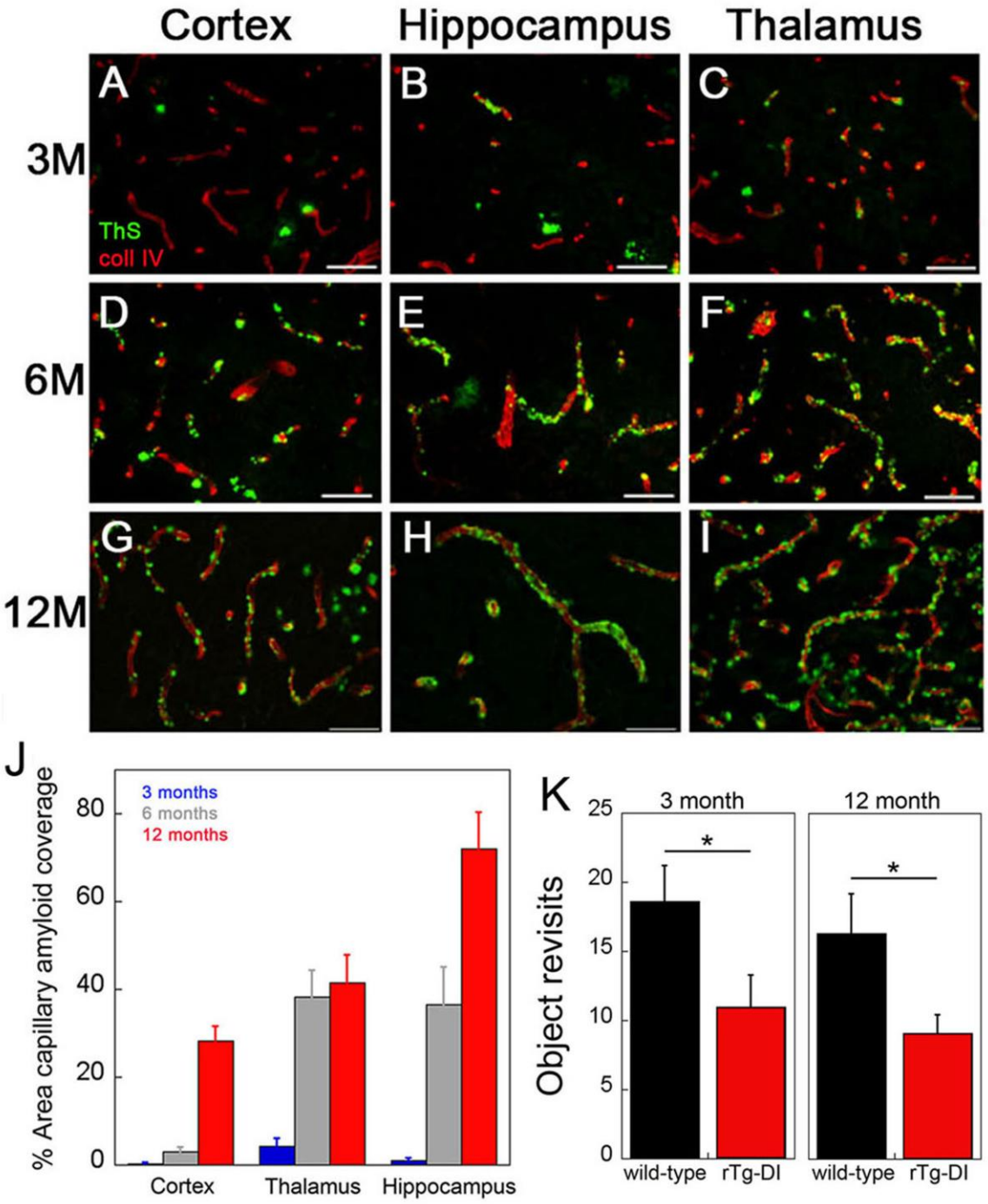
Cortex
Hippocampus
Thalamus
A
B
C
3M
ThS
coll IV
D
E
F
6M
G
H
I
12M
J
3 months
6 months
12 months
% Area capillary amyloid coverage
0
20
40
60
80
Cortex
Thalamus
Hippocampus
K
3 month
12 month
Object revisits
0
5
10
15
20
25
*
*
wild-type
rTg-DI
wild-type
rTg-DI

Figure 3

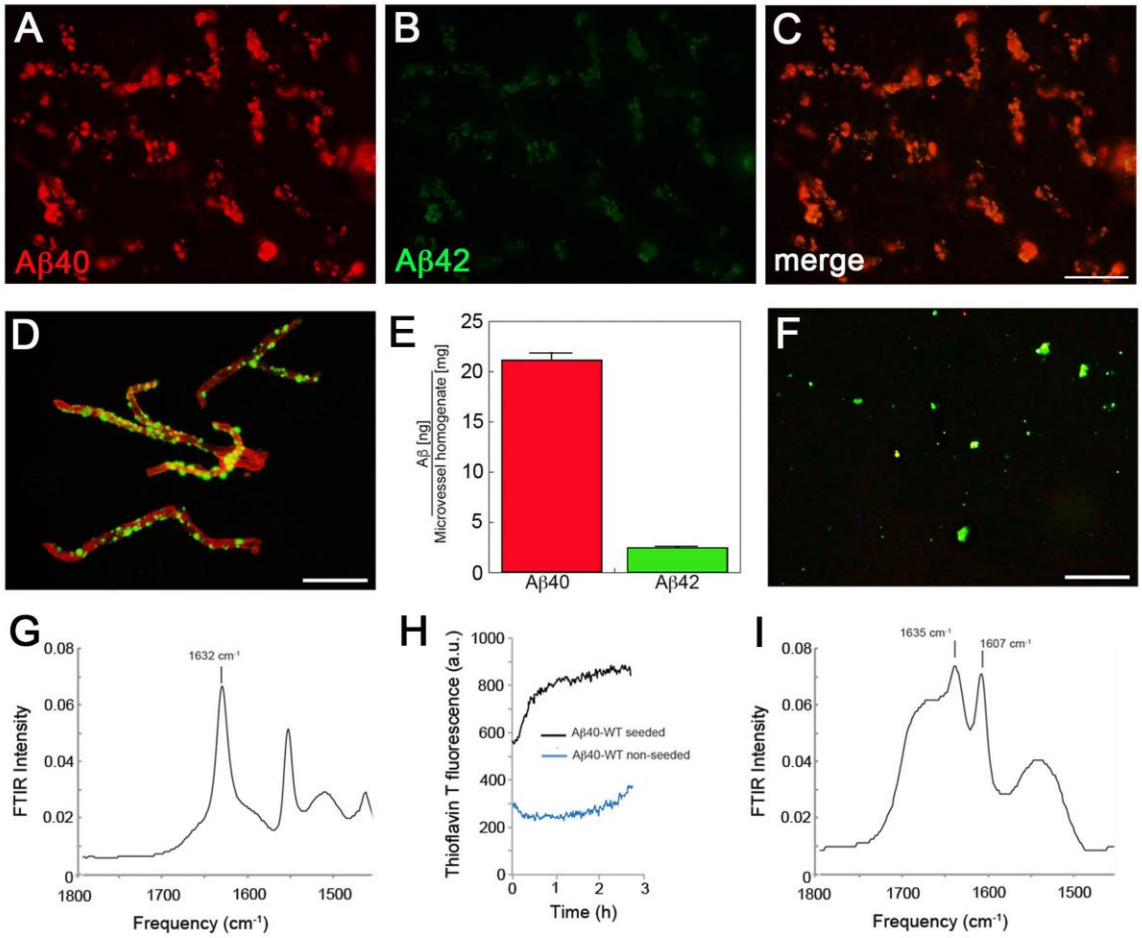
A
Aβ40
B
Aβ42
C
merge
D
E
Aβ [ng]
Microvessel homogenate [mg]
25
20
15
10
5
0
Aβ40
Aβ42
F
G
FTIR Intensity
0.08
0.06
0.04
0.02
0
1632 cm⁻¹
1800
1700
1600
1500
Frequency (cm⁻¹)
H
Thioflavin T fluorescence (a.u.)
1000
800
600
400
200
0
Aβ40-WT seeded
Aβ40-WT non-seeded
0
1
2
3
Time (h)
I
FTIR Intensity
0.08
0.06
0.04
0.02
0
1635 cm⁻¹
1607 cm⁻¹
1800
1700
1600
1500
Frequency (cm⁻¹)

Figure 4

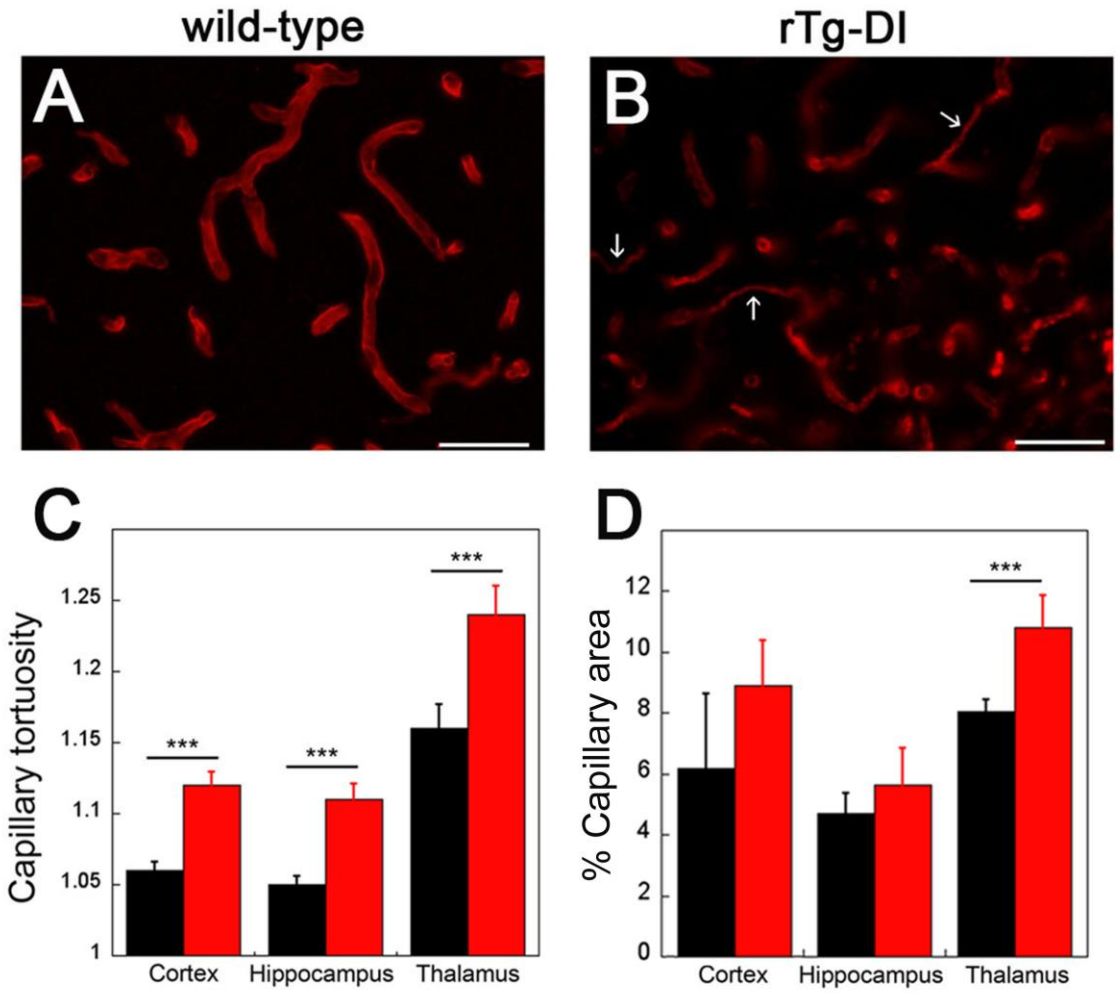
wild-type
rTg-DI
A
B
C
D
Capillary tortuosity
1.25
1.2
1.15
1.1
1.05
1
***
***
***
Cortex
Hippocampus
Thalamus
% Capillary area
12
10
8
6
4
2
0
***
Cortex
Hippocampus
Thalamus

Figure 5

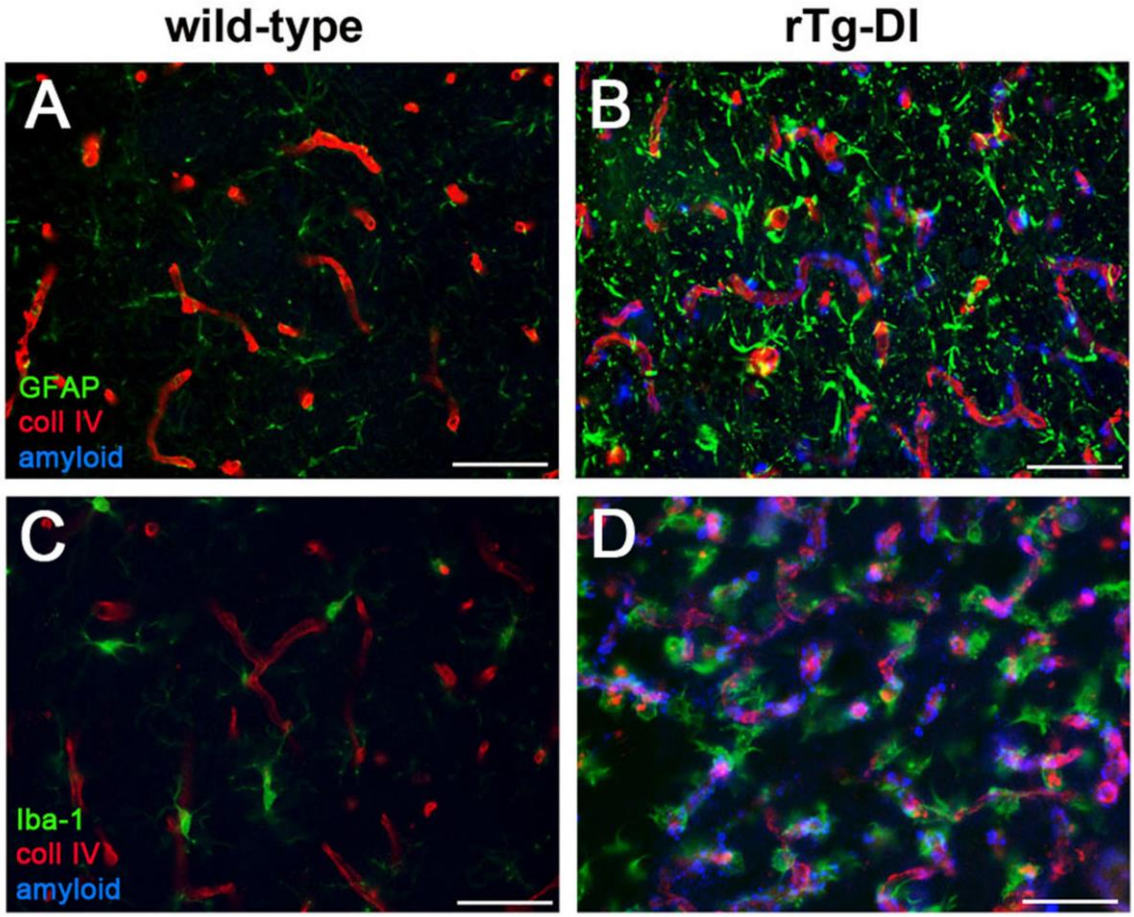
wild-type
rTg-DI
A
B
GFAP
coll IV
amyloid
C
D
Iba-1
coll IV
amyloid

Figure 6

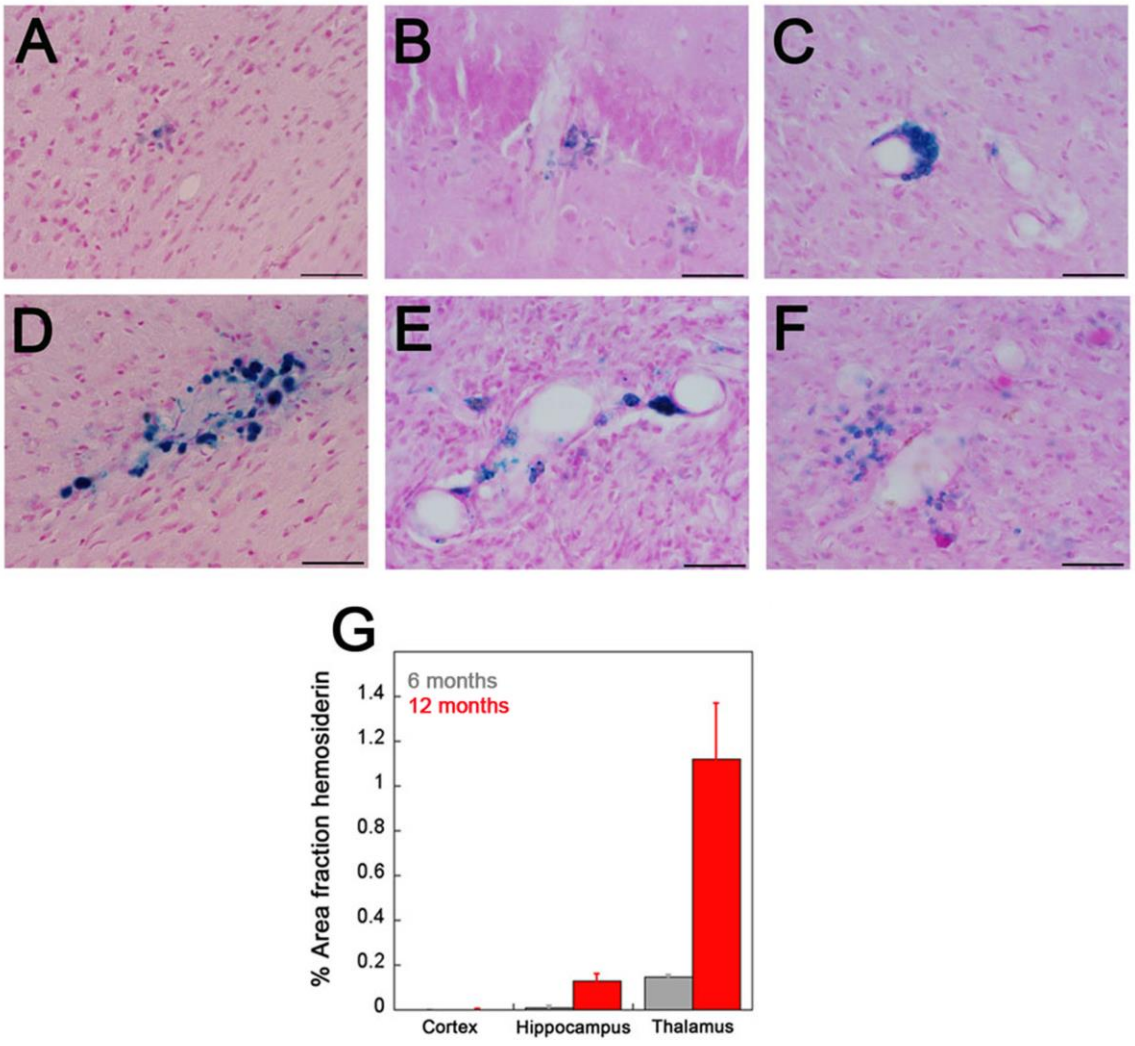
A
B
C
D
E
F
G
6 months
12 months
% Area fraction hemosiderin
1.4
1.2
1
0.8
0.6
0.4
0.2
0
Cortex
Hippocampus
Thalamus

Figure 7

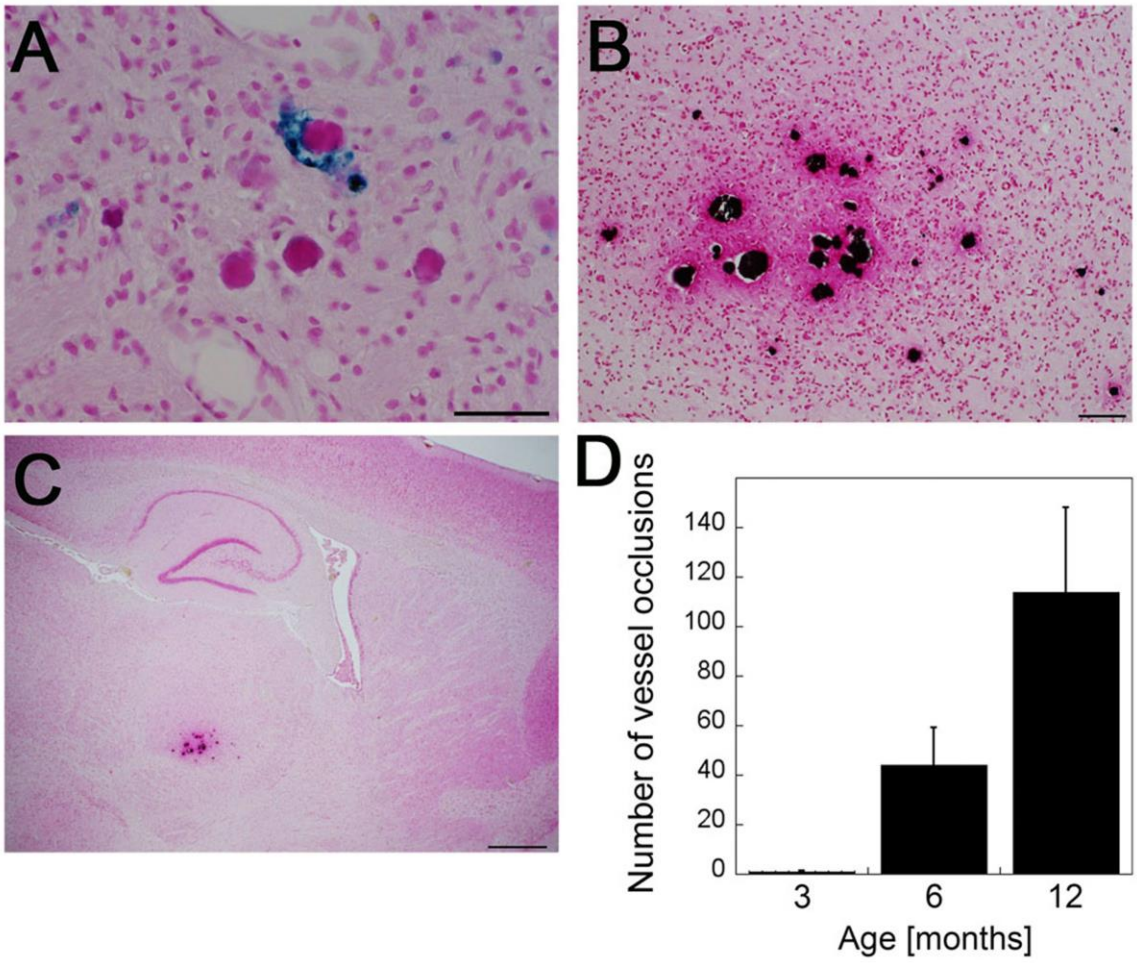
A
B
C
D
Number of vessel occlusions
0
20
40
60
80
100
120
140
3
6
12
Age [months]

Figure 8

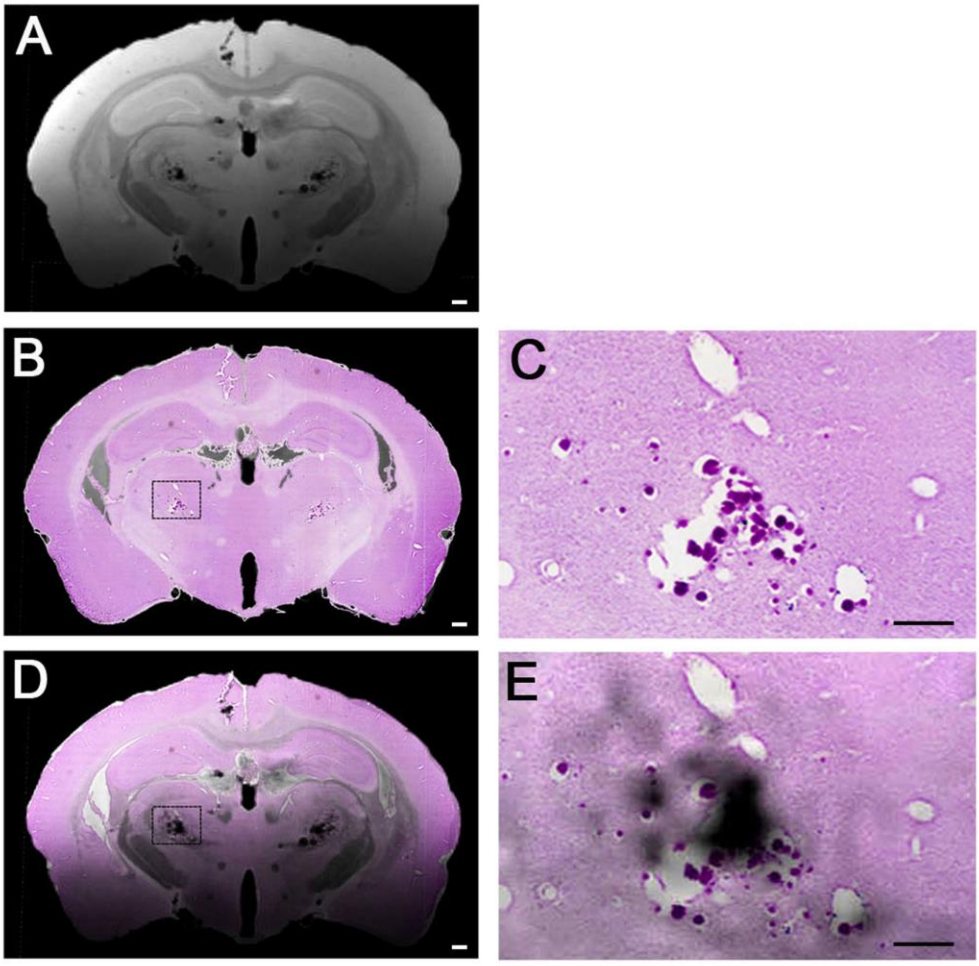
A
B
C
D
E

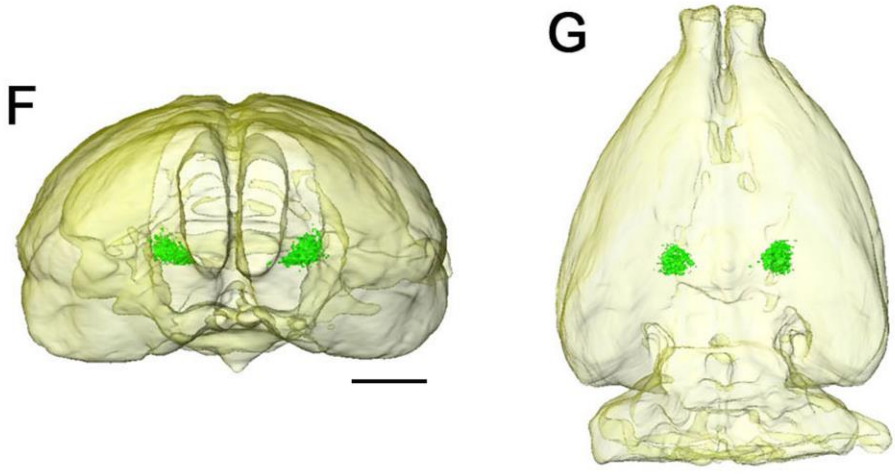
F
G